# [1]Supplementary Information for

## A molecular imprinted SERS sensor based on a silver substrate for the selective capture and sensitive detection of crystal violet in textile wastewater

Xiaohui Ren[a, *], Kailai Zhang[a], Jiaying Dou[a], Fei Xue[a], Xinyu Liu[a], Chenhui Yin[b], Wenjie Ma[a,**]

*a. College of Textile and Clothing, Yancheng Institute of Technology, Yancheng 224051, China*

*b. School of Chemistry and Chemical Engineering, Yangzhou University, Yangzhou, 225002, China*

[1]

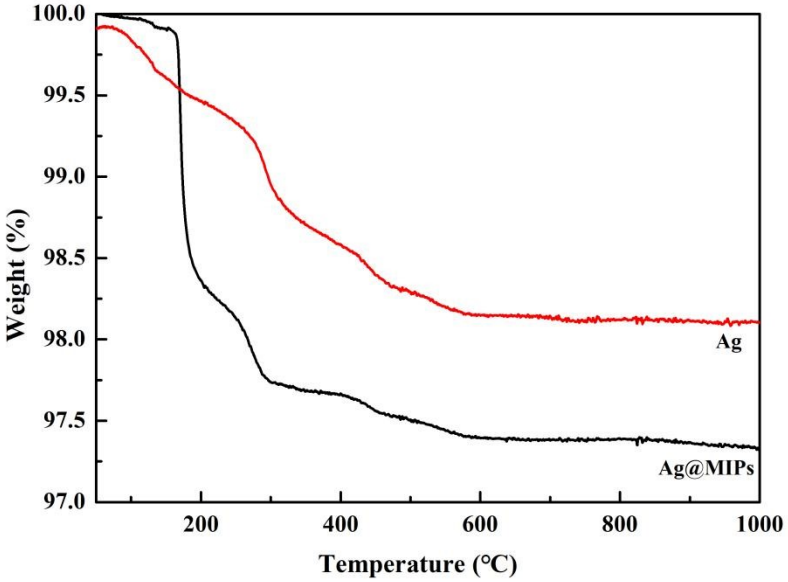


Fig. S1 The TGA curves of Ag and Ag@MIPs.

The enhancement factor (EF) = $(I_{SERS}/C_{SERS})/(I_{RS}/C_{RS})$ was used to obtain the EF of Ag@MIPs/Ag[S1-S4]. Among them, the $C_{Ag@MIPs}$ ($1.0\times10^{-15}$ mol $L^{-1}$) and $C_{Ag}$($1.0\times10^{-11}$mol $L^{-1}$) represents the lowest concentration of crystal violet. The $I_{Ag@MIPs}$ and $I_{Ag}$ represents the SERS intensity of crystal violet under Ag@MIPs and Ag as SERS substrate, respectively. Thus, the EF of 1619 $cm^{-1}$ Raman peak is estimated to be $1.12\times10^{4}$. The enhancement factor (EF) = $(I_{SERS}/C_{SERS})/(I_{RS}/C_{RS})$ was used to obtain the EF of Ag@MIPs[S1-S4]. Among them, $C_{SERS}$ ($1.0\times10^{-15}$ mol $L^{-1}$) and $C_{RS}$ ($1.0\times10^{-8}$ mol $L^{-1}$) represents the lowest concentration of crystal violet. The $I_{SERS}$ represent the SERS intensity of crystal violet under Ag@MIPs as SERS substrate. And $I_{RS}$ is the Raman intensity of crystal violet under non-SERS substrate. Thus, the EF of 1619 $cm^{-1}$ Raman peak is estimated to be $4.42\times10^{6}$. In summary, it indicated the excellent SERS performance for crystal violet detection by Ag@MIPs as SERS substrate.

## References


[S1] J.Y. Qiu, Y.J. Chu, Q.H. He, Y.K. Han, Y. Zhang, L. Han, A self-assembly hydrophobic oCDs/Ag nanoparticles SERS sensor for ultrasensitive melamine detection in milk, Food Chem. 402 (2023) 134241

[S2] S. Guo, S. Wang, L. Wang, T.F. Jiao, M.L. Wang, Sensitive metal-enhanced photoluminescence and Raman scattering magnetic core-shell nano-particles with tunable size for the detection of methylene blue, Opt. & Laser Tech. 181 (2025) 112061.

[S3] S. Guo, H.J. Cao, Y.F. Yang, M.L. Wang, Silver nanoparticles modified on cicada wings affect fluorescence and Raman signals based on electromagnetic and chemical enhancement mechanisms, Opt. & Laser Tech. 181 (2025) 111912.

[S4] V. Sharma and V. Krishnan, Fabrication of highly sensitive biomimetic SERS substrates for detection of herbicides in trace concentration, Sensor. Actuat. B 262 (2018) 710-719.

The comparison of analytical results of this method and other methods found in the literature for the determination of crystal violet or other dyes were shown in Table S1. The parameters of analytical range and minimum detection concentration of this method was comparable or superable to other methods. Compared with high performance liquid chromatography and UV-Vis spectrophotometer methods, SERS methods has outstanding advantages such as highly sensitive, time-saving without tedious sample preparation process and wide applications. In addition, compared with other SERS method, the molecular imprinting technique used in this method has high selectivity, excellent stability and good reproducibility.

Table S1 Comparison of this method with other methods used in the literature

| Methods | Materials | Analytes | Analytical ranges (mol $L^{-1}$) | Minimum detection concentration (mol $L^{-1}$) | Analysis time (min) | LOD (mol $L^{-1}$) | LOQ (mol $L^{-1}$) | Advantages | Ref. |
|---|---|---|---|---|---|---|---|---|---|
| HPLC-DAD | molecularly imprinted SPE | crystal violet | $0\text{-}5.4\times10^{-7}$ (0-200 μg/L ) | - | 8 | $2.7\times10^{-10}$(0.1 μg/L) 0.05 μg/kg | $9.5\times10^{-10}$ (0.35 μg/L) 0.17 μg/kg | good selectivity and affinity | S5 |
| UV-Vis | corn-silk doped molecularly imprinted polymer | crystal violet | $1.3\times10^{-5}$-$5.35\times10^{-4}$ (5-200 mg/L) | - | Timely response | - | - | highly selective and effective, economically feasible | S6 |
| HPLC-DAD | molecularly imprinted solid-phase extraction | crystal violet | $0\text{-}5.4\times10^{-7}$ (0-200 μg/L) | - | 8 | - | - | good selectivity and affinity | S7 |
| LC/MS/MS | molecularly imprinted polymer | acid green 16 | $5\times10^{-6}$-$2.40\times10^{-4}$ | - | - | - | - | great efficiency, high selectivity, good affinity | S8 |
| UV-Vis | magnetic imprinted polymer-based quartz crystal microbalance | methylene blue | $7.8\times10^{-8}$-$4.7\times10^{-7}$ ($25\text{-}1.5\times10^{2}$ μg/L) | - | Timely response | $4.4\times10^{-9}$ (1.4 μg/L) | - | good sensitivities, rapid responses, and lack of need for label mean | S9 |
| SERS | gold colloids | crystal violet | $1.3\times10^{-9}$-$2.7\times10^{-7}$ (0.5-100 ng/mL) | $1.3\times10^{-9}$ (0.5 ng/mL) | Timely response | $1.7\times10^{-8}$ (6.45 ng/g) | - | higher sensitivity and better quantitative analysis results | S10 |
| SERS | silver nanowires | crystal violet malachite green | - | $2.45\times10^{-11}$ (0.01 ng/mL ) $1.0\times10^{-10}$ (0.05 ng/mL ) | Timely response | - | - | high sensitivity and activity, cost-efficient, relatively good reproducibility | S11 |
| SERS | $Fe_3O_4$@PEI@Ag | Malachite green, crystal violet, et al. | $1\times10^{-1}$- $1\times10^{-8}$ $1\times10^{-1}$- $1\times10^{-10}$ | $1\times10^{-18}$ $1\times10^{-10}$ | Timely response | $3.6\times10^{-10}$ $4.0\times10^{-11}$ | - | superior enhancement factor, dual functionality, and excellent discrimination capabilities | S12 |
| SERS | Ag@MIPs | crystal violet | $1.0\times10^{-15}$ -$1.0\times10^{-3}$ | $1.0\times10^{-15}$ | Timely response | $2.75\times10^{-15}$ | $2.78\times10^{-15}$ | high selectivity, satisfactory sensitive, considerable anti-interference ability, excellent stability | This work |

## References


[S5] Z.R. Lian, J.T. Wang, Determination of crystal violet in seawater and seafood samples through off-line molecularly imprinted SPE followed by HPLC with diode-array detection, J. Sep. Sci, 36 (2013) 980-985.

[S6] K.N. Awokoya, V.O. Oninla, G.O. Akindoyin, A.T. Famojuro, E.G. Fakola, A.A.T. Taleat, A.O. Ogunfowokan, Experimental and computational studies on corn-silk doped molecular imprinted polymer for the sequestration of crystal violet from aqueous solution, Ife Journal of Science, 26 (2024) 259-275.

[S7] Z.R. Lian, J.T. Wang, Molecularly imprinted polymers for selective extraction of crystal violet from natural seawater coupled with highperformance liquid chromatographic determination, J. Ocean Univ. China 13 (2014) 236-242.

[S8] M.V. Foguel, N.T.B. Pedro, A. Wong, S. Khan, M. Valnice, B. Zanoni, M.P.T. Sotomayor, Synthesis and evaluation of a molecularly imprinted polymer for selective adsorption and quantification of Acid Green 16 textile dye in water sample, Talanta 170 (2017) 244-251.

[S9] Y.F. Hu, H.W. Xing, G. Li, M.H. Wu, Magnetic imprinted polymer-based quartz crystal microbalance sensor for sensitive label-free detection of methylene blue in groundwater, Sensors 20 (2020) 5506.

[S10] C.Y. Li, Y.Q. Huang, L. Pei, W.H. Wu, W.S. Yu, B.A. Rasco, K.Q. Lai, Analyses of trace crystal violet and leucocrystal violet with gold nanospheres and commercial gold nanosubstrates for surface-enhanced Raman spectroscopy, Food Anal. Methods 7 (2014) 2107-2112.

[S11] J. Song, Y.Q. Huang, Y.X. Fan, Z.H. Zhao, W.S. Yu, B.A. Rasco, K.Q. Lai, Detection of prohibited fish drugs using silver nanowires as substrate for surface-enhanced Raman scattering, Nanomaterials 6 (2016) 175.

[S12] D. Kumar, A.K. Yadav, A. Yadav, S. Rani, P. Kumar, D. Dixit, S. Gupta, Kang, S.N. Chen, X. Li, Versatile hybrid magnetic core silver-shell ($Fe_3O_4$@PEI@Ag) microspheres based SERS substrates for detection of organic dyes pollutant, J. Mol. Struct. 1322 (2025) 140522.

Table S2 Data on RSD, uncertainty, and statistical error for the reusability of Ag@MIPs.

| | **RSD（%）** | **U(*k*=2, Confidence Level=95%) (Counts)** | **$U_r$ (%)** | **RSE (%)** |
|---|---|---|---|---|
| 911 $cm^{-1}$ | 10.22 | $1.04\times10^3$ | 10.70 | -3.13 |
| 1176 $cm^{-1}$ | 9.72 | $1.28\times10^3$ | 9.60 | -7.57 |
| 1619 $cm^{-1}$ | 12.50 | $2.23\times10^3$ | 11.97 | 6.47 |

Ag microspheres were fabricated via a self-assembly approach. The rough surface morphology of these microspheres enables strong electromagnetic field coupling, which further enhances the SERS effect. A MIP layer was coated on the surface of the spherical Ag particles, and the thickness of this MIP layer was found to significantly influence the SERS enhancement. An excessively thin MIP layer fails to ensure the uniformity of imprinted cavities, while an overly thick layer compromises the electromagnetic enhancement effect of the silver core on template molecules. In this study, the thickness of the MIP layer was controlled within the range of 5-50 nm, which is consistent with previous literature reports indicating that MIP layers with thicknesses between 2-40 nm can effectively generate electromagnetic-enhanced Raman signals[S13-S15]. Compared with the SERS enhancement performance of silver microspheres, the Ag@MIPs composites exhibited superior SERS activity due to the presence of numerous imprinted cavities within the MIP layer. The SERS enhancement mechanism was elucidated using the "hot spot" theory, which posits that nanogaps and/or junctions between metal particles or structures generate localized electromagnetic hot spots that dramatically amplify SERS signals. Specifically, a small fraction of template molecules adsorbed at these hot spots contributes disproportionately to the overall SERS enhancement. Based on this hypothesis, the enhanced SERS activity of Ag@MIPs composites is attributed to the preferential formation of imprinted cavities within the plasmonic hot spots of the MIP layer. To verify this assumption, Raman mapping images of silver microspheres and Ag@MIPs composites were acquired at the characteristic peaks of 911 $cm^{-1}$ and 1619 $cm^{-1}$. As shown in Fig.R1, distinct hot spots were clearly observed in the Raman mapping images. Compared with silver microspheres, the Ag@MIPs composites displayed stronger signal intensities in the Raman mapping images, indicating the formation of more hot spots. Additionally, the experimental results revealed that the Raman mapping intensity at 1619 $cm^{-1}$ was higher than that at 911 $cm^{-1}$, which is consistent with the corresponding SERS spectra. These findings confirm that SERS enhancement arises not only from the plasmon resonance of the nanostructure but also

from the imprinted cavities within the MIP layer. Another contributing factor to the enhanced SERS performance is the specific adsorption of template molecules by the imprinted cavities in the MIP layer. This specific adsorption increases the signal-to-noise ratio (SNR), thereby promoting SERS enhancement. In summary, the remarkable SERS enhancement of Ag@MIPs composites is attributed to the synergistic effect of electromagnetic enhancement and chemical enhancement.

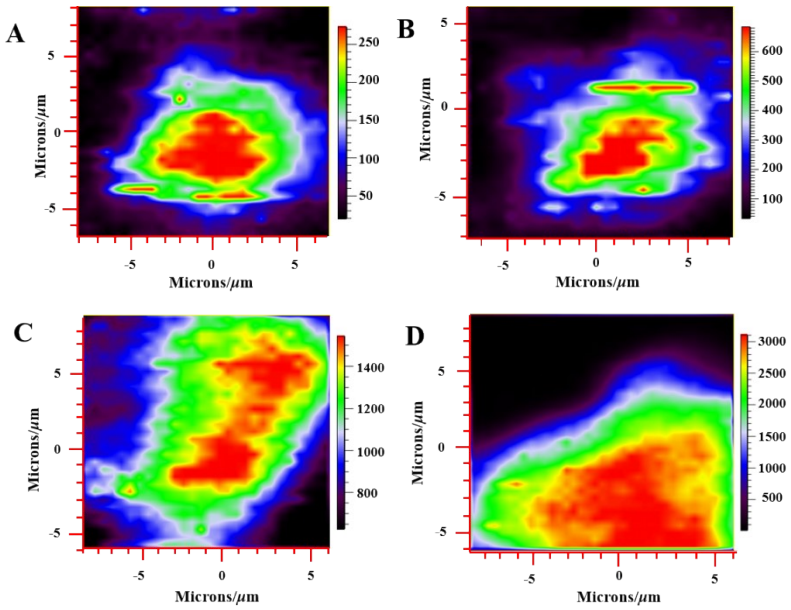


Fig. S2 The Raman mapping images of Ag particles (A and B), and Ag@MIPs (C and D)(the characteristic peaks at 911 $cm^{-1}$ (A and C) and 1619 $cm^{-1}$ (B and D)).

## References

[S13] L.M. Chang, Y. Ding, X. Li, Biosens. Bioelectron., 2013, 50, 106-110.

[S14] Y. Guo, L. L. Kang, S. N. Chen and X. Li, Phys. Chem. Chem. Phys., 2015, 17,21343-21347.

[S15] Z.G. Liu, Y. Gao, L. Jin, H. Jin, N. Xu, X.Y. Yu and S.H. Yu, ACS Sustainable Chem. Eng. 2019, 7, 8168-8175.

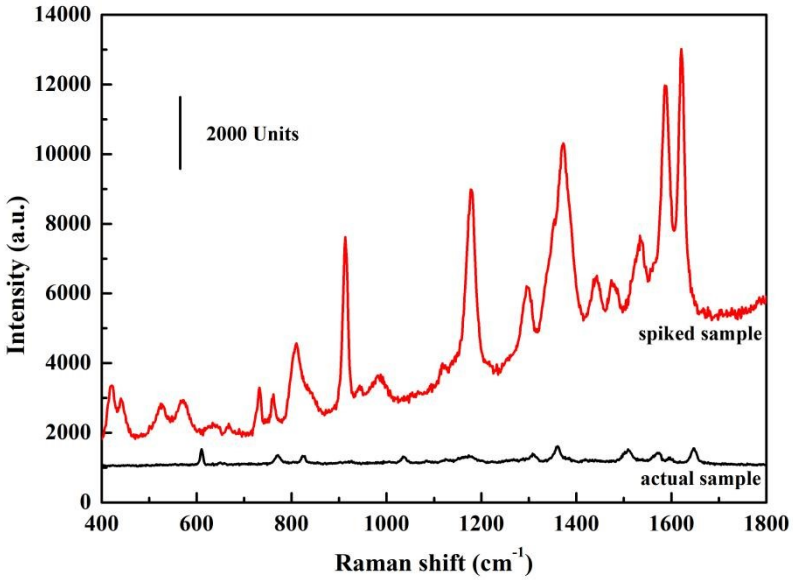


Fig. S3 The SERS spectrum of actual sample with and without CV ($1.0\times10^{-11}$ mol $L^{-1}$).

Table S3 Application of Ag@MIPs for quantitation of CV in waster sample and fish (n= 3).

| | Add (mol $L^{-1}$) | Found (mol $L^{-1}$) | Recovery (%) | RSD (%) |
|---|---|---|---|---|
| water sample | $1.0\times10^{-11}$ | $0.985\times10^{-11}\pm0.021$ | 98.5 | 2.13 |
| | $1.0\times10^{-9}$ | $0.989\times10^{-9}\pm0.036$ | 98.9 | 3.64 |
| | $1.0\times10^{-7}$ | $1.002\times10^{-7}\pm0.043$ | 100.2 | 4.29 |
| fish | $1.0\times10^{-11}$ | $0.967\times10^{-11}\pm0.032$ | 96.7 | 3.22 |
| | $1.0\times10^{-9}$ | $0.997\times10^{-9}\pm0.047$ | 99.7 | 4.71 |
| | $1.0\times10^{-7}$ | $1.005\times10^{-7}\pm0.028$ | 100.5 | 2.85 |

Taking the characteristic peak at 1619 $cm^{-1}$ as an example, the calculation method for the LOD is as follows: 1. Measure 10 blank samples (samples without analytes) and calculate the average detection value ($y_0$) and standard deviation (SD). 2. Use the negative logarithm of concentration as the X-coordinate and the detected Raman signal intensity as the Y-coordinate, the fitted linear equation is Y=48792.8-3343.0X, thus obtaining the slope k and intercept b. 3. Based on $y=y_0+3SD$, -log C=(y-b)/k, and C=10^(-(y-b)/k), the LOD value is calculated to be $2.75\times10^{-15}$ mol $L^{-1}$.

Taking the characteristic peak at 1619 $cm^{-1}$ as an example, the calculation method for the LOQ is as follows: 1. Measure 10 blank samples (samples without analytes) and calculate the average detection value ($y_0$) and standard deviation (SD). 2. Use the negative logarithm of concentration as the X-coordinate and the detected Raman signal intensity as the Y-coordinate, the fitted linear equation is Y=48792.8-3343.0X, thus obtaining the slope k and intercept b. 3. Based on $y=y_0+10SD$, -log C=(y-b)/k, and C=10^(-(y-b)/k), the LOQ value is calculated to be $2.78\times10^{-15}$ mol $L^{-1}$.